

Cation- and lattice-site-selective magnetic depth profiles of ultrathin $\text{Fe}_3\text{O}_4(001)$ films

Tobias Pohlmann,^{1,2,*} Timo Kuschel,³ Jari Rodewald,¹ Jannis Thien,¹ Kevin Ruwisch,¹ Florian Bertram,² Eugen Weschke,⁴ Padraic Shafer,⁵ Joachim Wollschläger,^{1,†} and Karsten Küpper^{1,‡}

¹*Department of Physics, Osnabrück University, Barbarastr. 7, 49076 Osnabrück, Germany*

²*DESY Photon Science, Notkestr. 85, 22607 Hamburg, Germany*

³*Center for Spinelectronic Materials and Devices, Department of Physics, Bielefeld University, Universitätsstr. 25, 33615 Bielefeld, Germany*

⁴*Helmholtz-Zentrum Berlin für Materialien und Energie,*

Wilhelm-Conrad-Röntgen-Campus BESSY II, Albert-Einstein-Strasse 15, 12489 Berlin, Germany

⁵*Advanced Light Source, Lawrence Berkeley National Laboratory, 6 Cyclotron Rd, Berkeley, CA, 94720, USA*

(Dated: May 5, 2020)

A detailed understanding of ultrathin film surface properties is crucial for the proper interpretation of spectroscopic, catalytic and spin-transport data. We present x-ray magnetic circular dichroism (XMCD) and x-ray resonant magnetic reflectivity (XRMR) measurements on ultrathin Fe_3O_4 films to obtain magnetic depth profiles for the three resonant energies corresponding to the different cation species $\text{Fe}_{\text{oct}}^{2+}$, $\text{Fe}_{\text{tet}}^{3+}$ and $\text{Fe}_{\text{oct}}^{3+}$ located on octahedral and tetrahedral sites of the inverse spinel structure of Fe_3O_4 . By analyzing the XMCD spectrum of Fe_3O_4 using multiplet calculations, the resonance energy of each cation species can be isolated. Performing XRMR on these three resonant energies yields magnetic depth profiles that correspond each to one specific cation species. The depth profiles of both kinds of Fe^{3+} cations reveal a 3.9 ± 1 Å-thick surface layer of enhanced magnetization, which is likely due to an excess of these ions at the expense of the $\text{Fe}_{\text{oct}}^{2+}$ species in the surface region. The magnetically enhanced $\text{Fe}_{\text{tet}}^{3+}$ layer is additionally shifted about 3 ± 1.5 Å farther from the surface than the $\text{Fe}_{\text{oct}}^{3+}$ layer.

Introduction.—Magnetite, Fe_3O_4 , is one of the most frequently investigated transition-metal oxides, since it is a key material in spintronics [1], spin caloritronics [2] and material chemistry [3]. Fe_3O_4 thin films were considered highly suitable as electrode material for magnetic tunnel junctions [4, 5] due to their predicted half-metallic behavior with 100% spin polarization [6]. However, the promise was never quite met, with modest tunnel magnetoresistance ratios ranging from -26% to 18% [4, 5, 7]. In order to test its half-metallicity, spin-resolved x-ray photoelectron spectroscopy on $\text{Fe}_3\text{O}_4(111)$ films found a spin-polarization of about 80% [8], while on $\text{Fe}_3\text{O}_4(001)$ the same technique yielded polarizations of only $\approx 40\% - 70\%$ [9–11].

Both the reduced tunnel magnetoresistance and the deviations from 100% spin-polarization in spin-resolved XPS were argued to emerge from interface and surface effects, respectively [4, 5, 8, 10, 11]. For $\text{Fe}_3\text{O}_4(111)$ films deposited on semiconducting $\text{ZnO}(0001)$, lattice-site-selective depth profiles obtained by x-ray resonant magnetic reflectivity (XRMR) and electron energy loss spectroscopy did not find a notable surface modification apart from a Fe_{oct} termination [12]. Reduction of the spin-polarization measured at the $\text{Fe}_3\text{O}_4(001)$ surface was typically considered to originate from a surface reconstruction, the existence of which has long been known but only recently has been resolved as a subsurface cation vacancy (SCV) structure [13]. This revelation highlights the issues that might arise from generalizing results from surface-sensitive techniques, such as x-ray absorption spectroscopy (XAS) in total electron yield (TEY) mode and x-ray photoelectron spectroscopy

(XPS), to explain the behavior of the bulk material [14].

In particular, drawing conclusions about the cation distribution of magnetite requires caution, because the bulk material of the inverse spinel Fe_3O_4 should contain divalent $\text{Fe}_{\text{oct}}^{2+}$, as well as trivalent ions in both octahedral and tetrahedral coordination, $\text{Fe}_{\text{tet}}^{3+}$ and $\text{Fe}_{\text{oct}}^{3+}$. However, the DFT+U calculations of the SCV structure predict the first four atomic layers to only contain Fe^{3+} ions and to have a formal stoichiometry of $\text{Fe}_{11}\text{O}_{16}$, in agreement with earlier reports on an excess of Fe^{3+} at the (001) surface [15]. A subsequent study of how the magnetic properties of Fe_3O_4 are affected at the surface used x-ray magnetic circular dichroism (XMCD) with varying probing depth and found a reduced magnetic moment at the surface of a natural magnetite crystal [16].

In this letter we report an investigation of the magnetic surface properties of ultrathin $\text{Fe}_3\text{O}_4(001)$ films, in contrast to the bulk, by recording magneto-optical depth profiles of the three cation species in Fe_3O_4 . Using photons with resonant energies, we employed XRMR to determine the magneto-optical depth profiles at the energies characteristic for $\text{Fe}_{\text{oct}}^{2+}$, $\text{Fe}_{\text{tet}}^{3+}$ and $\text{Fe}_{\text{oct}}^{3+}$ in magnetite's $L_{2,3}$ XMCD spectrum individually for three ultrathin $\text{Fe}_3\text{O}_4/\text{MgO}(001)$ films of varying thicknesses. We find a ≈ 3.9 Å layer of enhanced magneto-optical absorption at the surface at the resonant energies of both Fe^{3+} species but not for Fe^{2+} , suggesting an Fe^{3+} -rich surface.

Experimental and theoretical details.—We prepared the $\text{Fe}_3\text{O}_4/\text{MgO}(001)$ samples in a multichamber ultrahigh-vacuum system using reactive molecular beam epitaxy (RMBE). Their chemical composition and $(\sqrt{2} \times \sqrt{2})\text{R}45^\circ$ superstructure was confirmed by *in-situ*

XPS and low-energy electron diffraction (LEED), respectively. For details on the deposition and characterization methods please see Refs. [17] or [18].

For the XAS and XMCD study, the samples were transferred from our lab under ambient conditions to the Superconducting Vector Magnet Endstation at beamline 4.0.2 of the Advanced Light Source (ALS). All samples were measured in a magnetic field of 4 T along the x-ray beam at room temperature. The incidence angle of the x-rays was 30° from the [100] direction of Fe_3O_4 , and the degree of circular polarization was 90%. The XAS and XMCD spectra were measured across the Fe $L_{2,3}$ absorption edges (690 – 750 eV). All XAS spectra were measured in the TEY mode, which has a probing depth in magnetite of about 3 nm.

The XAS and XMCD data were analyzed by applying the sum rules [19–21] and charge-transfer multiplet calculations using the Thole code [22] with assistance of CTM4XAS [23, 24]. For the sum rules, we took into account a correction factor of 1.142 derived by Teramura *et al.* for Fe^{2+} [21] and assumed $14 \frac{\text{holes}}{\text{f.u.}}$. For the multiplet calculations, we assumed the three-cation model, using crystal field and charge-transfer parameters as described in Ref. [17]. The parameters and more details regarding the multiplet calculations can also be found in the Supplemental Materials [25] (Chapter A, including Refs. [17, 26, 27]). The multiplet states resulting from these calculations were compared to the data by assuming a Gaussian instrumental broadening of 0.2 eV, and a Lorentzian lifetime broadening of 0.3 eV at L_3 and 0.6 eV at L_2 .

The samples were transferred to BESSY II under ambient conditions and x-ray reflectivity (XRR) and XRMR were performed in the XUV Diffractometer at beamline UE46_PGM-1 [28]. The samples were placed between two permanent magnets in a magnetic field of 200 mT at room temperature, with a degree of circular polarization of 90%. First, we characterized the structural properties of the sample (thickness d , roughness σ) by XRR at off-resonant energies (680 eV, 1000 eV). Second, XAS and XMCD were measured in order to select suitable energies for XRMR. Finally, $\theta - 2\theta$ scans in the range $2\theta = 0^\circ - 140^\circ$ at resonant energies E_i with extrema in the XMCD signal (maximum at 708.4 eV, minimum at 709.5 eV, maximum at 710.2 eV) were performed with both right and left circularly polarized x-rays, to obtain the XRMR asymmetry ratios $\Delta I(E_i, q_z)$. These curves were then fitted with the Zak matrix formalism using the software ReMagX [29] to determine the depth profiles of the magneto-optical absorption $\Delta\beta(z)$ and dispersion $\Delta\delta(z)$ along the film height z . A detailed review of the XRMR method and the software is given in Ref. [29], and a conclusive recipe for fitting XRMR data can be found in Refs. [30, 31].

Results.—Structural parameters obtained from the off-resonant XRR measurements are displayed in Tab. I.

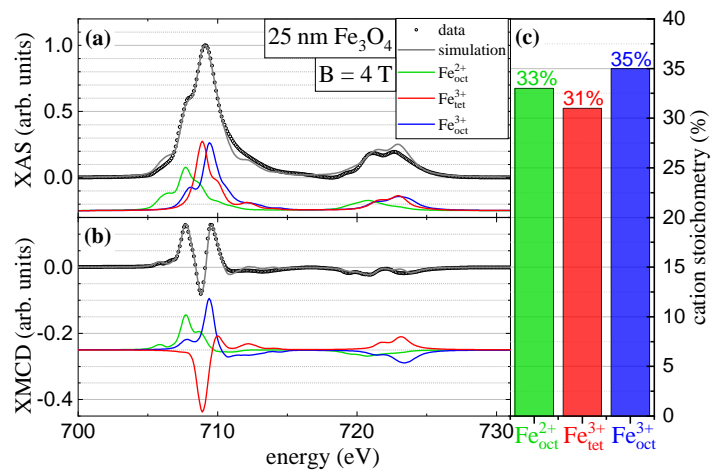


FIG. 1. (a) XAS and (b) XMCD spectrum at the Fe $L_{2,3}$ edge for the 25 nm Fe_3O_4 film, taken at 4 T external magnetic field, at room temperature and in TEY mode. A step function was subtracted from the XAS spectrum. Black dots represent data; green, red and blue spectra are multiplet calculations for the three cation species of Fe_3O_4 , the grey line is their sum. The cation spectra are offset for better visibility. (c) Cation stoichiometry used to obtain the fit in (a) and (b).

Figure 1 shows the XAS and XMCD spectra of the 25 nm Fe_3O_4 film, recorded at ALS. Corresponding data measured at BESSY II, under the same conditions in which the XRMR was performed, can be found in the Supplemental Material [25] (Chapter A). The spin and orbital moments μ_{spin} and μ_{orb} obtained from the sum rules are given in Tab. I. Their sum is slightly reduced compared to the bulk value of magnetite of $\mu = \mu_{\text{spin}} + \mu_{\text{orb}} = 4.07 \mu_B$ [32]. They also show a tendency toward a slightly higher moment for the thicker films. This behavior of magnetite films has also been observed previously [17], and can be explained by a higher density of anti-phase boundaries (APBs) for thinner films due to the antiferromagnetic coupling of APBs reducing the average magnetic moment of the film [33–35].

Additionally, multiplet simulations of the three-cation model are fitted to the XMCD data (cf Fig. 1). By

TABLE I. Thicknesses d , surface roughnesses σ^{surf} and interface roughnesses σ^{int} of the investigated samples as obtained by fitting off-resonant XRR curves, as well as their spin moments μ_{spin} and orbital moments μ_{orb} from the sum-rule analysis.

sample	13 nm	25 nm	50 nm
d (nm)	13.5 ± 0.5	25.2 ± 0.3	52.8 ± 0.3
σ^{surf} (nm)	0.22 ± 0.05	0.33 ± 0.05	0.34 ± 0.05
σ^{int} (nm)	0.35 ± 0.05	0.35 ± 0.05	0.37 ± 0.05
μ_{spin} ($\mu_B/\text{f.u.}$)	3.2 ± 0.3	3.5 ± 0.3	3.7 ± 0.3
μ_{orb} ($\mu_B/\text{f.u.}$)	0.07 ± 0.02	0.09 ± 0.02	0.11 ± 0.02
μ ($\mu_B/\text{f.u.}$)	3.27 ± 0.3	3.59 ± 0.3	3.81 ± 0.3

weighting the individual spectra with respect to the cation stoichiometry given in Fig. 1(c), the XAS and XMCD data can be described well by our model (cf. grey line). Thus, the cation distribution on different sites almost follows the ideal stoichiometry of 1:1:1.

One feature of this kind of modelling is the fact that each of the three extrema observed in the XMCD spectrum can mainly be attributed to one cation spectrum. Table II shows the contributions $r^{\text{cation}}(E_i)$ of each cation spectrum at the resonant energies E_i in the XMCD spectrum, according to

$$r^{\text{cation}}(E_i) = \frac{I^{\text{cation}}(E_i)}{|I^{\text{Fe}_{\text{oct}}^{2+}}(E_i)| + |I^{\text{Fe}_{\text{tet}}^{3+}}(E_i)| + |I^{\text{Fe}_{\text{oct}}^{3+}}(E_i)|}, \quad (1)$$

with $I^{\text{cation}}(E_i)$ being the XMCD signal of the corresponding cation spectrum in Fig. 1(b) at energies $E_i = 708.4 \text{ eV}$, 709.5 eV , 710.2 eV . While there still is a considerable mixing, at least 64% of each extremum can be attributed to its dominant cation.

The distinction between the $\text{Fe}_{\text{oct}}^{2+}$ and $\text{Fe}_{\text{oct}}^{3+}$ ions is a noteworthy issue for several reasons. Above the Verwey transition temperature, these ions should be randomly distributed on octahedral sites as shown by neutron diffraction [36]. Thus, the model could potentially be simplified by describing them as $\text{Fe}_{\text{oct}}^{2.5+}$, effectively reducing the number of cation species. However, only multiplet calculations based on a three-cation model describe room-temperature spectra from XPS, XAS and XMCD at the Fe L absorption edge with sufficient agreement [17, 37–40]. Note that this extremum-cation assignment qualitatively also holds true in LSDA+U calculations, but they predict a stronger overlap of the three cation spectra [41]. A possible explanation for this behavior may well be the different electronic structure at the surface of magnetite. In that case, we would expect different spectra from the surface and the bulk. In fact, a recent study using hard x-ray photoelectron spectroscopy (HAXPES) reported on a bulk-exclusive state not observable in surface-sensitive soft XPS [42].

Accordingly, the strategy to obtain cationic depth profiles is to pick the three corresponding XMCD resonant energies and perform XRMR measurements at these resonances. Figure 2 shows the asymmetry ratios and their fits at the three XMCD resonant energies for the 25 nm Fe_3O_4 film. Corresponding figures for the other

TABLE II. Contributions of the three cation species to the extrema in the XMCD spectrum in Fig. 1(b), as obtained by the multiplet analysis using Eq. (1).

Energy	$\text{Fe}_{\text{oct}}^{2+}$	$\text{Fe}_{\text{tet}}^{3+}$	$\text{Fe}_{\text{oct}}^{3+}$
708.4 eV	$73 \pm 5\%$	$-8 \pm 3\%$	$19 \pm 5\%$
709.5 eV	$18 \pm 3\%$	$-64 \pm 3\%$	$18 \pm 3\%$
710.2 eV	$4 \pm 3\%$	$-16 \pm 8\%$	$80 \pm 10\%$

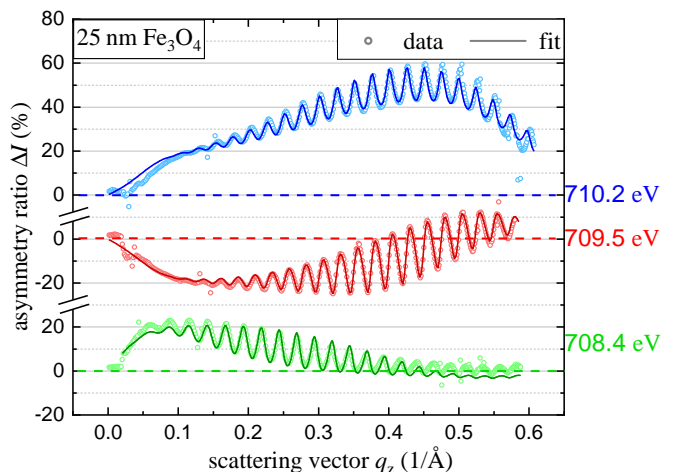


FIG. 2. XRMR data (open circles) and corresponding fits (solid lines) from the 25 nm Fe_3O_4 film, recorded at the three resonant energies of the XMCD L_3 edge, using the modeled magneto-optical depth profiles of Fig. 3(a). Data were recorded with a magnetic field of 200 mT along the $\text{Fe}_3\text{O}_4(001)$ direction at room temperature.

two samples can be found in the Supplemental Material [25] (Chapter B). The magneto-optical depth profiles $\Delta\beta(z)$ that produce the fits are shown in Fig. 3(a). The most striking feature of all three samples is the behavior at the surface: at the $\text{Fe}_{\text{oct}}^{2+}$ resonance energy (708.4 eV, green), the magneto-optical depth profiles in fact appear to be just homogeneous for all samples. However, at both the $\text{Fe}_{\text{tet}}^{3+}$ and the $\text{Fe}_{\text{oct}}^{3+}$ resonance energies, there are noticeable changes to the $\Delta\beta$ depth profiles. In order to fit their asymmetry ratios, we must include a thin surface layer of enhanced magneto-optical absorption. The two thinner Fe_3O_4 films - 13 nm and 25 nm - are quantitatively very similar for the $\text{Fe}_{\text{oct}}^{3+}$ and $\text{Fe}_{\text{tet}}^{3+}$ magneto-optical depth profiles, with only minor differences in the enhanced amplitude at the surface, and the $\Delta\beta$ in the bulk matches between the samples. In contrast, the 50 nm Fe_3O_4 film shows slightly higher $\Delta\beta$ at the $\text{Fe}_{\text{oct}}^{3+}$ resonance, and smaller $\Delta\beta$ at the $\text{Fe}_{\text{tet}}^{3+}$ resonance. Also, the magneto-optical absorption at the $\text{Fe}_{\text{oct}}^{2+}$ resonance becomes larger with increasing film thickness, in agreement with our results from the sum-rule analysis (see Tab. I). The obvious choice of magneto-optical depth profiles which are simply homogeneous through the entire film did not provide satisfactory fits to the data. This is discussed in more detail in the Supplemental Material [25] (Chapter C).

In order to highlight this phenomenon, Fig. 3(b) shows the surface region of the 25 nm Fe_3O_4 film, together with the density depth profile obtained from off-resonant RRR (grey line). The edge of the magneto-optical depth profile of the $\text{Fe}_{\text{oct}}^{2+}$ resonance roughly matches the location of the magnetically enhanced $\text{Fe}_{\text{tet}}^{3+}$ layer. The thickness of the magnetically enhanced layers is about 3.5 Å for both

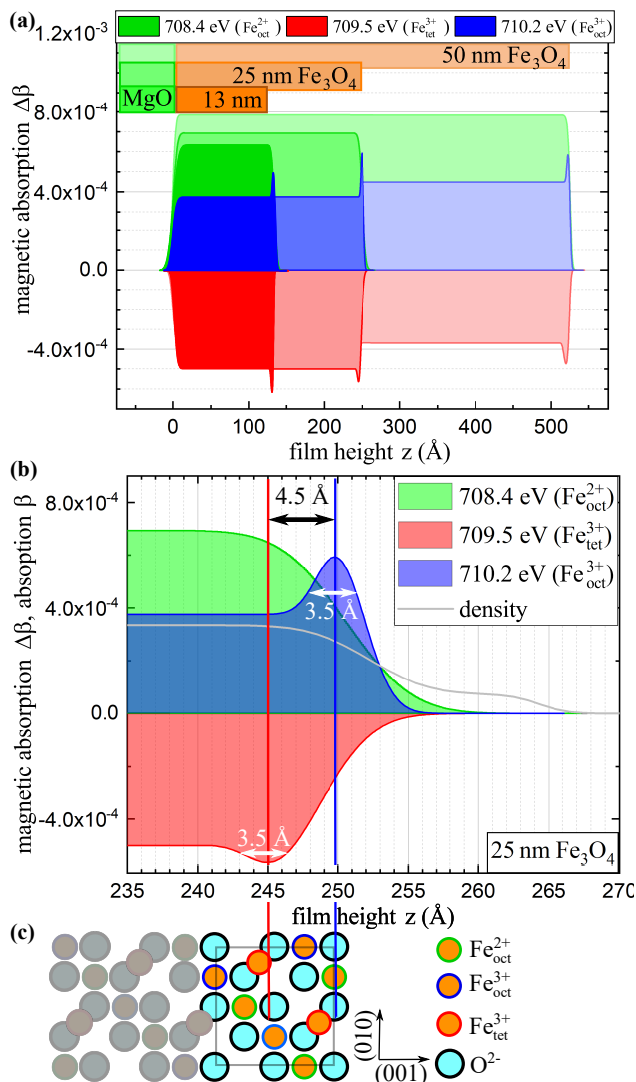


FIG. 3. (a) $\Delta\beta(z)$ depth profiles for all three samples at the three resonant energies, extracted from the XRMR fits. (b) Close-up of the surface magneto-optical depth profile of the 25 nm Fe_3O_4 film, together with the optical density obtained from off-resonant XRR fits (grey line). (c) (Bulk-terminated) model of the magnetite unit cell, in scale with Fig. 3(b). Comparison with the model in (c) illustrates the sizes of the enhanced regions being roughly half a unit cell of magnetite (four cation layers).

Fe^{3+} species. This corresponds to slightly less than half a bulk unit cell of magnetite ($a/2 = 4.2 \text{ \AA}$), as illustrated by Fig. 3(c). Furthermore, the magnetically enhanced layers are not collocated at the same depth: the magnetically enhanced $\text{Fe}_{\text{tet}}^{3+}$ layer is shifted about 4.5 \AA deeper into the film than the magnetically enhanced $\text{Fe}_{\text{oct}}^{3+}$ layer. Table III summarizes the individual thicknesses of the magnetically enhanced layers d^{enh} and their offset from one another for the different samples. All three samples show comparable, but not quite identical results. While the model qualitatively holds up well among the sam-

TABLE III. Thicknesses d^{enh} and vertical shifts of the enhanced magnetic layers at the $\text{Fe}_{\text{tet}}^{3+}$ and $\text{Fe}_{\text{oct}}^{3+}$ resonances.

	$d_{\text{Fe}_{\text{oct}}^{3+}}^{\text{enh}}$	$d_{\text{Fe}_{\text{tet}}^{3+}}^{\text{enh}}$	vertical shift
13 nm	4.7 \AA	3.2 \AA	2 \AA
25 nm	3.5 \AA	3.4 \AA	4.5 \AA
50 nm	3.8 \AA	6.4 \AA	2.5 \AA

ples, both the thicknesses d^{enh} and the depth offsets are similar in magnitude to the surface roughness, making it difficult to resolve the exact distances with any greater precision.

Discussion.—Within the three-cation picture, we can discuss the magneto-optical depth profiles obtained for the resonant energies. The magneto-optical depth profiles are not identical with the depth distribution of the cations: As quantified in Tab. II, however, the signal on each resonance is a mixture of contributions from all three cations. For the magneto-optical depth profile at 710.2 eV approximately 80% of the signal originates from the $\text{Fe}_{\text{oct}}^{3+}$ and can be regarded as an almost pure effect from that species. And since the position of the layer of enhanced magnetization at 709.5 eV does not match the position of the 710.2 eV layer, we can conclude it to be a distinct physical feature, stemming from the $\text{Fe}_{\text{tet}}^{3+}$ species.

One ansatz is to take into account rearranged cation distributions due to the $\text{Fe}_3\text{O}_4(001)$ surface as proposed by the SCV model [13, 14]. The SCV model predicts that, in order to achieve polarity compensation, the first unit cell contains only Fe^{3+} species, with the first $\text{Fe}_{\text{tet}}^{3+}$ layer lying about 1 \AA deeper than the $\text{Fe}_{\text{oct}}^{3+}$. This model matches surprisingly well some aspects of our findings. The first $\text{Fe}_{\text{oct}}\text{-O}$ layer remains stoichiometric, but the $\text{Fe}_{\text{oct}}^{2+}$ changes valency to $\text{Fe}_{\text{oct}}^{3+}$, effectively doubling the $\text{Fe}_{\text{oct}}^{3+}$ density. In the second layer, an additional $\text{Fe}_{\text{tet}}^{3+}$ ion is added, increasing the $\text{Fe}_{\text{tet}}^{3+}$ density by 50%. However, we do not observe the depletion of $\text{Fe}_{\text{oct}}^{2+}$ cations in the first 8.4 \AA . This agreement is surprising because Fe_3O_4 surfaces tend to hydroxylate on ambient conditions and do not show the $(\sqrt{2} \times \sqrt{2})R45^\circ$ LEED pattern, but instead a (1×1) pattern [14]. This, however, may be attributed to disorder at the surface with loss of long-range order while the local order of vacancies and interstitials is kept. Our results now suggest that at least the Fe^{3+} -enrichment of the surface remains intact under ambient conditions. A more detailed comparison of the SCV model to our findings can be found in the Supplemental Material [25] (Chapter D).

Taking the model of occupation of octahedral sites by $\text{Fe}_{\text{oct}}^{2.5+}$ cations as an alternative, the agreement of the XAS/XMCD spectra with the multiplet calculations might be merely valid at the surface, while both octahedrally coordinated Fe species are identical in the bulk. In

that case, the discrepancy between surface and bulk of the magneto-optical depth profiles would represent the transition from the surface electronic structure to the bulk structure. Using bulk-sensitive HAXPES, Taguchi *et al.* report on a bulk feature at 708.5 eV, which is invisible for surface-sensitive soft XPS [42]. In this picture, we could interpret the magneto-optical depth profiles and the XMCD spectra as follows: the top 4–6 Å, consisting of $\text{Fe}_{\text{oct}}^{3+}$ and $\text{Fe}_{\text{tet}}^{3+}$ ions, give rise to the XMCD extrema at 709.5 eV and 710.2 eV, as reflected in the enhanced $\Delta\beta$ layers at those energies. Deeper into the Fe_3O_4 film, the $\text{Fe}_{\text{oct}}^{3+}$ species vanishes in favor of the $\text{Fe}_{\text{oct}}^{2.5+}$ species, and consequently, the magnetic dichroism at 710.2 eV is reduced. Instead, the bulk-feature at 708.4 eV becomes prominent, related to the $\text{Fe}_{\text{oct}}^{2.5+}$ species. In the XMCD signal, it is visible as the supposed $\text{Fe}_{\text{oct}}^{2+}$ peak, but strongly suppressed due to the surface sensitivity of the TEY detection. In this interpretation, our results agree with the more pronounced signal at 708.5 eV far from the surface reported in Ref. [42], and can explain the observation of the two distinct Fe_{oct} species at the surface, which should not be distinguishable at room temperature.

Summary.—In conclusion, we fabricated three $\text{Fe}_3\text{O}_4/\text{MgO}(001)$ ultrathin films of different thicknesses by RMBE. We recorded XAS/XMCD at ALS beamline 4.0.2 as well as XAS/XMCD and XRMR measurements at BESSY II beamline UE46.PGM-1, in order to obtain magneto-optical depth profiles. By fitting multiplet calculations to the XMCD data, we disentangle the cation contributions at the three resonant energies of the XMCD spectrum, and use XRMR at those energies in order to resolve the magneto-optical depth profiles of the three iron species in Fe_3O_4 . We find that both Fe^{3+} species show an enhanced signal in the surface-near region in a $\approx 3.9 \pm 1$ Å thick layer, with the $\text{Fe}_{\text{tet}}^{3+}$ layer located about 3 ± 1.5 Å underneath the $\text{Fe}_{\text{oct}}^{3+}$ layer. We attribute this to the first unit cell from the surface containing an excess of Fe^{3+} cations.

Acknowledgements.—Financial support from the Bundesministerium für Bildung und Forschung (FKZ 05K16MP1) is gratefully acknowledged. We are also grateful for the kind support from the Deutsche Forschungsgemeinschaft (DFG under No. KU2321/6-1, and No. WO533/20-1). This research used resources of the Advanced Light Source, a DOE Office of Science User Facility under contract no. DE-AC02-05CH11231, by recording XMCD at beamline 4.0.2. (ALS-10261). We thank HZB for the allocation of synchrotron beamtime at beamline UE46.PGM-1 (181/06266ST/R) where we recorded the XRMR and additional XMCD measurements.

-
- * tobias.pohlmann@desy.de
† jwollsch@uni-osnabrueck.de
‡ kkuepper@uni-osnabrueck.de
- [1] J.-B. Moussy, *Journal of Physics D: Applied Physics* **46**, 143001 (2013).
 - [2] R. Ramos, T. Kikkawa, K. Uchida, H. Adachi, I. Lucas, M. H. Aguirre, P. Algarabel, L. Morelln, S. Maekawa, E. Saitoh, and M. R. Ibarra, *Applied Physics Letters* **102**, 072413 (2013).
 - [3] M. Lin and H. Leu, *Electroanalysis* **17**, 2068 (2005).
 - [4] T. Kado, *Applied Physics Letters* **92**, 092502 (2008).
 - [5] L. Marnitz, K. Rott, S. Niehörster, C. Klewe, D. Meier, S. Fabretti, M. Witzki, A. Krampf, O. Kuschel, T. Schemme, K. Kuepper, J. Wollschläger, A. Thomas, G. Reiss, and T. Kuschel, *AIP Advances* **5**, 047103 (2015).
 - [6] Z. Zhang and S. Satpathy, *Phys. Rev. B* **44**, 13319 (1991).
 - [7] G. Hu and Y. Suzuki, *Phys. Rev. Lett.* **89**, 276601 (2002).
 - [8] Y. S. Dedkov, U. Rüdiger, and G. Güntherodt, *Phys. Rev. B* **65**, 064417 (2002).
 - [9] J. G. Tobin, S. A. Morton, S. W. Yu, G. D. Waddill, I. K. Schuller, and S. A. Chambers, *Journal of Physics: Condensed Matter* **19**, 315218 (2007).
 - [10] M. Fonin, Y. S. Dedkov, R. Pentcheva, U. Rüdiger, and G. Güntherodt, *Journal of Physics: Condensed Matter* **20**, 142201 (2008).
 - [11] W. Wang, J.-M. Mariot, M. C. Richter, O. Heckmann, W. Ndiaye, P. De Padova, A. Taleb-Ibrahimi, P. Le Fèvre, F. Bertran, F. Bondino, E. Magnano, J. Krempaský, P. Blaha, C. Cacho, F. Parmigiani, and K. Hricovini, *Phys. Rev. B* **87**, 085118 (2013).
 - [12] S. Brück, M. Paul, H. Tian, A. Müller, D. Kufer, C. Praetorius, K. Fauth, P. Audehm, E. Goering, J. Verbeeck, G. Van Tendeloo, M. Sing, and R. Claessen, *Applied Physics Letters* **100**, 081603 (2012).
 - [13] R. Bliem, E. McDermott, and G. S. Parkinson, *Science* **346** (2014).
 - [14] G. S. Parkinson, *Surface Science Reports* **71**, 272 (2016).
 - [15] S. Chambers and S. Joyce, *Surface Science* **420**, 111 (1999).
 - [16] L. Martín-García, R. Gargallo-Caballero, M. Monti, M. Foerster, J. F. Marco, L. Aballe, and J. de la Figuera, *Phys. Rev. B* **91**, 020408 (2015).
 - [17] K. Kuepper, O. Kuschel, N. Pathé, T. Schemme, J. Schmalhorst, A. Thomas, E. Arenholz, M. Gorgoi, R. Ovsyannikov, S. Bartkowski, G. Reiss, and J. Wollschläger, *Phys. Rev. B* **94**, 024401 (2016).
 - [18] O. Kuschel, R. Buß, W. Spiess, T. Schemme, J. Wöllermann, K. Balinski, A. T. N'Diaye, T. Kuschel, J. Wollschläger, and K. Kuepper, *Phys. Rev. B* **94**, 094423 (2016).
 - [19] C. Piamteze, P. Miedema, and F. M. F. de Groot, *Phys. Rev. B* **80**, 184410 (2009).
 - [20] C. T. Chen, Y. U. Idzerda, H.-J. Lin, N. V. Smith, G. Meigs, E. Chaban, G. H. Ho, E. Pellegrin, and F. Sette, *Phys. Rev. Lett.* **75**, 152 (1995).
 - [21] Y. Teramura, A. Tanaka, and T. Jo, *Journal of the Physical Society of Japan* **65**, 1053 (1996).
 - [22] G. van der Laan, *Journal of Electron Spectroscopy and Related Phenomena* **86**, 41 (1997).
 - [23] F. de Groot, *Coordination Chemistry Reviews* **249**, 31

- (2005).
- [24] E. Stavitski and F. M. de Groot, *Micron* **41**, 687 (2010).
- [25] See Supplemental Material for details on the multiplet calculations, as well as those XMCD, XRR, and XRMR data which were not included in the main text. It also further illustrates the necessity to include the layers of enhanced magnetization in order to properly fit the XRMR data, and contains a thorough comparison of our model to the SCV model.
- [26] T. J. Regan, H. Ohldag, C. Stamm, F. Nolting, J. Lüning, J. Stöhr, and R. L. White, *Phys. Rev. B* **64**, 214422 (2001).
- [27] C. T. Chantler, *J. Phys. Chem Ref. Data* **24**, 71 (1995).
- [28] E. Weschke and E. Schierle, *Journal of large-scale research facilities* **4**, A127 (2018).
- [29] S. Macke and E. Goering, *Journal of Physics: Condensed Matter* **26**, 363201 (2014).
- [30] T. Kuschel, C. Klewe, J.-M. Schmalhorst, F. Bertram, O. Kuschel, T. Schemme, J. Wollschläger, S. Francoual, J. Strepfer, A. Gupta, M. Meinert, G. Götz, D. Meier, and G. Reiss, *Phys. Rev. Lett.* **115**, 097401 (2015).
- [31] C. Klewe, T. Kuschel, J.-M. Schmalhorst, F. Bertram, O. Kuschel, J. Wollschläger, J. Strepfer, M. Meinert, and G. Reiss, *Phys. Rev. B* **93**, 214440 (2016).
- [32] Weiss, Pierre and Forrer, R., *Ann. Phys.* **10**, 279 (1929).
- [33] S. Celotto, W. Eerenstein, and T. Hibma, *European Physical Journal B* **36**, 271 (2003).
- [34] A. V. Ramos, J.-B. Moussy, M.-J. Guittet, A. M. Bataille, M. Gautier-Soyer, M. Viret, C. Gatel, P. Bayle-Guillemaud, and E. Snoeck, *Journal of Applied Physics* **100**, 103902 (2006).
- [35] J.-B. Moussy, S. Gota, A. Bataille, M.-J. Guittet, M. Gautier-Soyer, F. Delille, B. Dieny, F. Ott, T. D. Doan, P. Warin, P. Bayle-Guillemaud, C. Gatel, and E. Snoeck, *Phys. Rev. B* **70**, 174448 (2004).
- [36] J. García, G. Subías, M. G. Proietti, H. Renevier, Y. Joly, J. L. Hodeau, J. Blasco, M. C. Sánchez, and J. F. Béjar, *Phys. Rev. Lett.* **85**, 578 (2000).
- [37] F. M. F. de Groot, J. C. Fuggle, B. T. Thole, and G. A. Sawatzky, *Phys. Rev. B* **42**, 5459 (1990).
- [38] P. Kuiper, B. G. Searle, L.-C. Duda, R. M. Wolf, and P. J. van der Zaag, *Journal of Electron Spectroscopy and Related Phenomena* **86**, 107 (1997).
- [39] P. S. Miedema and F. M. de Groot, *Journal of Electron Spectroscopy and Related Phenomena* **187**, 32 (2013).
- [40] D. Phase, G. Panchal, R. Rawat, S. Tiwari, R. Prakash, D. Jain, and R. Choudhary, *Journal of Magnetism and Magnetic Materials* **482**, 296 (2019).
- [41] V. N. Antonov, B. N. Harmon, and A. N. Yaresko, *Phys. Rev. B* **67**, 024417 (2003).
- [42] M. Taguchi, A. Chainani, S. Ueda, M. Matsunami, Y. Ishida, R. Eguchi, S. Tsuda, Y. Takata, M. Yabashi, K. Tamasaku, Y. Nishino, T. Ishikawa, H. Daimon, S. Todo, H. Tanaka, M. Oura, Y. Senba, H. Ohashi, and S. Shin, *Phys. Rev. Lett.* **115**, 256405 (2015).